Controllable hybrid shape of correlation and squeezing

Garuma Abdisa,[1] Irfan Ahmed,[1,2] Xiuxiu Wang,[1] Zongchen Liu,[1] Hongxing Wang,[1] and Yanpeng Zhang[1,*]

[1]*Key Laboratory for Physical Electronics and Devices of the Ministry of Education and Shaanxi Key Lab of Information Photonic Technique, Xi'an Jiaotong University, Xi'an 710049, China*

[2]*Electrical Engineering Department, Sukkur IBA, Sukkur 65200, Sindh, Pakistan*

(Received 10 November 2015; revised manuscript received 9 June 2016; published 29 August 2016)

Two- and three-mode correlation and squeezing of spontaneous parametric four-wave mixing (SPFWM) and fourth-order fluorescence (FL) composite signals are investigated theoretically and experimentally in both homonuclear (two-level) and heteronuclearlike (V-type level) molecular systems of Pr^{3+}:YSO. By selecting different time positions, changing the power, and changing the frequency detuning of the laser field, the competition between the composite signals is demonstrated. It is found that as the laser parameters change, the signal evolves from a nonlinear $\chi^{(4)}$ process resulting in a FL signal to a SPFWM signal ($\chi^{(3)}$ process). In addition, the competition effect between the signals determines the evolution of the shape of the correlation from a pure sharp to a two-stage (mixed) shape and finally to a pure broad peak amplitude. Furthermore, the signal evolution determines the magnitude of squeezing, which can control the noise level. Such progress may find potential applications in optical hybrid communication and information processing.

DOI: 10.1103/PhysRevA.94.023849

I. INTRODUCTION

The peculiarity of quantum correlations was shown by Einstein, Podolsky, and Rosen in their pioneering work in 1935 [1], which was later found to be important in quantum information processing [2]. The first experiment on the correlation between the intensity fluctuations recorded by two different detectors using a thermal light source was conducted by Hanbury-Brown and Twiss [3]. The late 1980s theoretical foundations [4,5] and recent works [6,7] thoroughly analyzed the impact of spectral properties of fields such as conservation of the commutation relation, generation of free fields, and impact on detected quantum correlations. The experimental manipulation of correlated photon pairs is of great interest for research in the emerging field of quantum information processing and long distance communication [8]. The correlated biphotons produced from the spontaneous parametric four-wave mixing (SPFWM) in Pr^{3+} : Y_2SiO_5 crystal demonstrates an "atomlike" property [9,10] with long coherence times (0.1–1 s) and narrow spectral width (∼MHz) as compared to the traditional spontaneous parametric downconversion process (∼THz). Thus the generation and control of Stokes (S) and anti-Stokes (aS) photon pairs using the SPFWM process has been achieved [11]. Moreover, the competition between SPFWM and fourth-order fluorescence (FL) [12] interference between two dressed multiwave mixing processes [13] and an electromagnetically induced lattice state [14] has been studied. Recently, entanglement between classical and nonclassical photons was identified as a useful resource for optical quantum information processing [15–17]. A hybrid entanglement (entanglement between two different types of states) has been demonstrated using the quantum mechanical single-photon state and the classical coherent state for efficient quantum information processing using the hybrid state as a new type of qubit [18].

In this paper, we study two-mode and three-mode intensity-noise correlation and intensity-difference squeezing of SPFWM and fourth-order FL composite signals. Manipulation of the broad and sharp peak amplitude of correlation and the magnitude of squeezing induced by dressed competition between the composite signals are investigated. A theoretical model is developed to explain the phenomena in homonuclear (two-level) and heteronuclearlike (V-type) three-level atomic systems. We showed that the shape of correlation and the magnitude of squeezing are determined by the dressed competition between the composite signals. The details are presented in the subsequent sections as follows: In Sec. II we show the experimental setup, in Sec. III, development of the theoretical model; in Sec. IV, experimental results and discussion; and finally in Sec. V we conclude the paper.

II. EXPERIMENTAL SETUP

A sample of 3-mm rare-earth-doped ($0.05\%Pr^{3+}$)Y_2SiO_5 (Pr:YSO) crystal is used in this experiment. In YSO crystal, dipole-dipole interaction enables the coupling between Pr^{3+} ions to be localized at different cation vacancies [19], which are labeled as δ_0 and γ_0 with and without an asterisk (*) for sites I and II, respectively, as shown in Fig. 1(a). The excited (triplet $^3H_4$) and ground (singlet $^1D_2$) states are split into nine and five Stark components, respectively, under the action of the crystal field of YSO. Since the two ion sites act as a heteronuclearlike molecule, we can construct two-level and V-type three-level atomic systems as shown in Fig. 1(a). Figure 1(b) shows the schematic diagram of the experimental setup. Two dye lasers (narrow scan with a 0.04-cm^{-1} linewidth) pumped by an injection locked single-mode Nd:YAG laser (Continuum Powerlite DLS 9010, 10-Hz repetition rate, 5-ns pulse width) are used to generate the pumping fields $E_1(\omega_1,\Delta_1)$ and $E_2(\omega_2,\Delta_2)$ with frequency detuning $\Delta_i = \Omega_{mn} - \omega_i$, where Ω_{mn} is the corresponding atomic transition frequency between levels $|m\rangle$ and $|n\rangle$. $\omega_i (i = 1,2)$ is the laser frequency. The pumping fields $E_1(\Delta_1,\omega_1)$ and $E_2(\Delta_2,\omega_2)$ satisfy the phase-matching condition $\mathbf{k_1} + \mathbf{k_2} = \mathbf{k_{Si}} + \mathbf{k_{aSi}}$, where $i = 1,2$ and $\mathbf{k}$ are the

*ypzhang@mail.xjtu.edu.cn

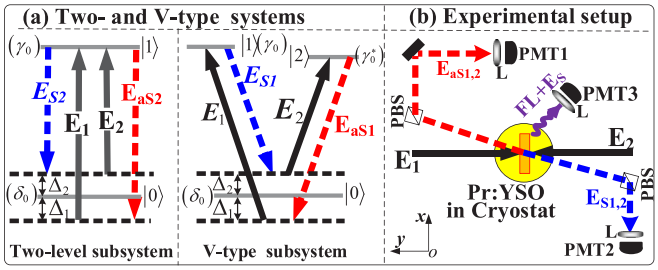

FIG. 1. (a) Two-level atomic system $[\delta_0(|0\rangle) \leftrightarrow \gamma_0(|1\rangle)]$ and three-level (V-type) atomic system $(|0\rangle(\delta_0) \leftrightarrow |1\rangle(\gamma_0)$ and $[|0\rangle(\delta_0) \leftrightarrow |2\rangle(\gamma_0^*)]$ in Pr^{3+}:YSO crystal and laser coupling configuration (b) experimental setup, where Δ_1, Δ_2 are frequency detunings of E_1 and E_2 fields, respectively $(\Delta_1 = \omega_{01} - \omega_1, \Delta_2 = \omega_{02} - \omega_2)$; PMT: photomultiplier tube; L: lens; PBS: polarizing beam splitter; E_S: Stokes signal; E_{aS}: anti-Stokes signal; FL: fluorescence signal; δ: ground-state energy levels; γ: excited-state energy levels (δ_0–$\gamma_0 = 602$ nm, δ_0–$\gamma_0^* = 609.24$ nm).

wave vectors of the pumping fields and the generated photon pairs. E_1 and E_2 are coupled to the transition $\delta_0(|0\rangle) \leftrightarrow \gamma_0(|1\rangle)$ and $\delta_0(|0\rangle) \leftrightarrow \gamma_0^*(|2\rangle)$, respectively. The laser beams are in the same plane, x-o-y, as shown in Fig. 1(b). Arrangements of three photomultiplier tubes (PMT1-3) are used to detect the generated E_S, E_{aS}, and FL composite signals [Fig. 1(b)]. The spectral signals are obtained by scanning laser frequency, while time domain signals are obtained by fixing laser frequency.

III. THEORETICAL MODEL

A. SPFWM and fourth-order FL in two-level and V-type three-level systems

Density-matrix elements of Stokes and anti-Stokes are derived using the Liouville equation $\frac{\partial \hat{\rho}(t)}{\partial t} = \frac{1}{i\hbar}[\hat{H}, \hat{\rho}(t)] - \Gamma\hat{\rho}$, where $\hat{H} = \hat{H}_0 + \hat{H}_1(t)$; $\hat{H}_0$ is the Hamiltonian of the free atom; and $H_1 = -E\vec{\mu}$, where $\vec{\mu}$ is the transition dipole moment. H is the Hamiltonian; Γ is the population decay rate. By adopting the perturbation theory to obtain the Stokes and anti-Stokes signals under the weak-field approximation (see the Appendix) and the strong pump field as a dressing field for the two-level system via $\rho_{00}^{(0)} \xrightarrow{E_1} \rho_{10}^{(1)} \xrightarrow{(E_{aS_2})^*} \rho_{00}^{(2)} \xrightarrow{E_2} \rho_{10(S_2)}^{(3)}$ and $\rho_{00}^{(0)} \xrightarrow{E_2} \rho_{10}^{(1)} \xrightarrow{(E_{S_2})^*} \rho_{00}^{(2)} \xrightarrow{E_1} \rho_{10(aS_2)}^{(3)}$ perturbation chains, and considering the dressing terms, one can write

$$\rho_{S_2}^{(3)} = \frac{-iG_{aS_2}^* G_1 G_2}{\left[\Gamma_{10} + i\Delta_1 + \frac{|G_1|^2}{\Gamma_{00}} + \frac{|G_2|^2}{\Gamma_{00}+i(\Delta_1-\Delta_2)}\right][\Gamma_{00} + i(\Delta_1 - \Delta_2)]} \frac{1}{\left[\Gamma_{10} + i\Delta_1 + \frac{|G_1|^2}{\Gamma_{00}} + \frac{|G_2|^2}{\Gamma_{00}+i(\Delta_1-\Delta_2)}\right]}, \tag{1}$$

$$\rho_{aS_2}^{(3)} = \frac{-iG_{S_2}^* G_1 G_2}{\left[\Gamma_{10} + i\Delta_2 + \frac{|G_1|^2}{\Gamma_{00}+i(\Delta_2-\Delta_1)} + \frac{|G_2|^2}{\Gamma_{00}}\right]^2 [\Gamma_{00} + i(\Delta_2 - \Delta_1)]}, \tag{2}$$

where $G_i = -\mu_{ij} E_i/\hbar$ is the Rabi frequency, μ_{ij} is the electric dipole moment between levels $|i\rangle$ and $|j\rangle$, and Γ_{ij} is the transverse decay rate. The FL signal is generated accompanying the SPFWM process and its intensity in the two-level system is proportional to the square of the diagonal elements of the density matrix. When $\boldsymbol{E}_1$ and $\boldsymbol{E}_2$ are open simultaneously, the fourth-order FL $\rho_{FL}^{(4)}$, which can be generated via the pathway $\rho_{00}^{(0)} \xrightarrow{E_2} \rho_{10}^{(1)} \xrightarrow{-E_2} \rho_{00}^{(2)} \xrightarrow{E_1} \rho_{10}^{(3)} \xrightarrow{-E_1} \rho_{00}^{(4)}$, is given as

$$\rho_{FL}^{(4)} = \frac{|G_2|^2}{(d_1' + |G_1|^2/d_{01} + |G_2|^2/\Gamma_{00})(\Gamma_{00} + |G_1|^2/d_1 + |G_2|^2/d_1')} \frac{|G_1|^2}{(d_1 + |G_1|^2/\Gamma_{00} + |G_2|^2/d_{01}')(\Gamma_{11} + |G_1|^2/d_1)}, \tag{3}$$

where $d_1' = \Gamma_{10} + i\Gamma_2$, $d_{01} = \Gamma_{00} + i(\Gamma_2 - \Gamma_1)$, $d_1 = \Gamma_{10} + i\Gamma_1$, and $d_{01}' = \Gamma_{00} + i(\Gamma_1 - \Gamma_2)$. Similarly, with the dressing perturbation theory, for a V-type three-level system with two strong pumping fields E_1 and E_2, taking the self-dressing effect of E_1 and the external dressing effect of E_2 into account, the third-order nonlinear density-matrix elements of E_{S_1} and E_{aS_1} obtained via the perturbation chain $\rho_{00}^{(0)} \xrightarrow{E_2} \rho_{20}^{(1)} \xrightarrow{-E_2} \rho_{00}^{(2)} \xrightarrow{E_1} \rho_{10(S_1)}^{(3)}$ and $\rho_{00}^{(0)} \xrightarrow{E_1} \rho_{10}^{(1)} \xrightarrow{-E_1} \rho_{00}^{(2)} \xrightarrow{E_2} \rho_{20(aS_1)}^{(3)}$ are given by

$$\rho_{S_1}^{(3)} = \frac{-iG_2^2 G_1}{\left(d_2 + \frac{|G_2|^2}{\Gamma_{00}} + \frac{|G_1|^2}{d_{21}}\right)\Gamma_{00}\left(d_1 + \frac{|G_2|^2}{d_{12}} + \frac{|G_1|^2}{\Gamma_{00}}\right)}, \tag{4}$$

$$\rho_{aS_1}^{(3)} = \frac{-iG_2 G_1^2}{\left(d_1 + \frac{|G_1|^2}{\Gamma_{00}} + \frac{|G_2|^2}{d_{12}}\right)\Gamma_{00}\left(d_2 + \frac{|G_1|^2}{d_{21}} + \frac{|G_2|^2}{\Gamma_{00}}\right)}, \tag{5}$$

where $d_2 = \Gamma_{20} + i\Delta_2$, $d_{21} = \Gamma_{21} + i(\Delta_2 - \Delta_1)$, $d_1 = \Gamma_{10} + i\Delta_1$, and $d_{12} = \Gamma_{12} + i(\Delta_1 - \Delta_2)$. The fluorescence signals FL1 from $|1\rangle$ to $|0\rangle$ and FL2 from $|2\rangle$ to $|0\rangle$ are generated simultaneously. The intensity of the total fluorescence signals is the sum of two signals described by the fourth-order coherence process via the pathways $\rho_{00}^{(0)} \xrightarrow{E_2} \rho_{20}^{(1)} \xrightarrow{-E_2} \rho_{00}^{(2)} \xrightarrow{E_1} \rho_{10}^{(3)} \xrightarrow{-E_1} \rho_{11}^{(4)}$ and $\rho_{00}^{(0)} \xrightarrow{E_1} \rho_{10}^{(1)} \xrightarrow{-E_1} \rho_{00}^{(2)} \xrightarrow{E_2} \rho_{20}^{(3)} \xrightarrow{-E_2} \rho_{22}^{(4)}$, respectively.

$$\rho_{FL_1}^{(4)} = \frac{|G_2|^2}{(d_2 + |G_2|^2/\Gamma_{00} + |G_1|^2/d_{21})(\Gamma_{11} + |G_1|^2/d_1)} \times \frac{|G_1|^2}{(d_1 + |G_1|^2/\Gamma_{00} + |G_2|^2/d_{12})(\Gamma_{00} + |G_1|^2/d_1 + |G_2|^2/d_2)}, \tag{6}$$

$$\rho_{FL_2}^{(4)} = \frac{-|G_1|^2}{(d_1 + |G_1|^2/\Gamma_{00} + |G_2|^2/d_{12})(\Gamma_{22} + |G_2|^2/d_2)} \times \frac{-|G_2|^2}{(d_2 + |G_2|^2/\Gamma_{00} + |G_1|^2/d_{21})(\Gamma_{00} + |G_1|^2/d_1 + |G_2|^2/d_2)}, \tag{7}$$

where $d_1 = \Gamma_{10} + i\Gamma_1$, $d_2 = \Gamma_{20} + i\Gamma_2$, $d_{12} = \Gamma_{12} + i(\Gamma_1 - \Gamma_2)$, and $d_{21} = \Gamma_{21} + i(\Gamma_2 - \Gamma_1)$. Equations (1)–(7) show that FL and SPFWM signals can be controlled by dressing fields. The intensity of temporal multi peaks [Eqs. (3), (6), and (7)] FL signals are determined by

$$I(t) = a_0 \exp\left(-G_a^2 t^2\right) + \rho \exp(-\Gamma_{\mathrm{FL}} t) + a_1 \exp\left[-(t - t_0)^2/2t_p^2\right] + a_2 \exp[-\Gamma(t - t_0)], \tag{8}$$

where $a_0 \exp(-G_a^2 t^2)$ is the FL signal intensity at the photoexcitation stage and G_a^2 is the Rabi frequency of the fields; $\rho \exp(-\Gamma_{\mathrm{FL}} t)$ is the FL signal intensity at zero delay stage, and Γ_{FL} is the decoherence rate; $a_1 \exp[-(t - t_0)^2/2t_p^2]$ is the FL signal intensity at the adiabatic population transition stage; and $a_2 \exp[-\Gamma(t - t_0)]$ is the FL signal at the spontaneous radiation stage. ρ in Eq. (8) can be $\rho_{\mathrm{FL}}^{(4)}$ in Eq. (3) or $\rho_{\mathrm{FL}_1}^{(4)}$ or $\rho_{\mathrm{FL}_2}^{(4)}$ in Eqs. (6) and (7).

B. Two-mode and three-mode correlation and squeezing

The coupling Hamiltonian for the SPFWM process is $H = (\hat{a}_{\mathrm{S}}^{\dagger}\hat{a}_{\mathrm{aS}}^{\dagger} + \hat{a}_{\mathrm{S}}\hat{a}_{\mathrm{aS}})g/v$, where $\hat{a}_{\mathrm{S}}^{\dagger}(\hat{a}_{\mathrm{S}})$ and $\hat{a}_{\mathrm{aS}}^{\dagger}(\hat{a}_{\mathrm{aS}})$ are creation and annihilation operators acting on Stokes and anti-Stokes signals, respectively, while v is the group velocity of the field in the nonlinear medium. The nonlinear gain $g = |(-i\omega_{Si,\mathrm{aS}i}\chi_{Si,\mathrm{aS}i}^{(3)}E_1E_2/2c|$, where $(i = 1,2)$, depends on the nonlinear susceptibility $\chi_{Si,\mathrm{aS}i}^{(3)}$ and the pumping field amplitude, where $\chi_{Si,\mathrm{aS}i}^{(3)} = (N\mu_{\mathrm{S,aS}}\rho_{Si,\mathrm{aS}i}^{(3)})/(\varepsilon_0 E_1 E_2 E_{Si,\mathrm{aS}i})$. The output photon number at each channel is given by $N_j = \langle\hat{a}_j^{+}\hat{a}_j\rangle$ and the corresponding intensity $I_j(t_j) = N_j \exp(-\Gamma_j t_j)$ $(j = \mathrm{S}_{1,2}, a\mathrm{S}_{1,2})$. Thus the respective intensity of the output Stokes and anti-Stokes signals proportional to the photon number is given by [12]

$$\langle\hat{a}_{\mathrm{S}}^{+}\hat{a}_{\mathrm{S}}\rangle = \frac{1}{2}\left[\cos\left(2t\sqrt{AB}\sin\frac{\varphi_1+\varphi_2}{2}\right) + \cosh\left(2t\sqrt{AB}\cos\frac{\varphi_1+\varphi_2}{2}\right)\right]\frac{A}{B}, \tag{9}$$

$$\langle\hat{a}_{\mathrm{aS}}^{+}\hat{a}_{\mathrm{aS}}\rangle = \frac{1}{2}\left[\cos\left(2t\sqrt{AB}\sin\frac{\varphi_1+\varphi_2}{2}\right) + \cosh\left(2t\sqrt{AB}\cos\frac{\varphi_1+\varphi_2}{2}\right)\right]\frac{B}{A}. \tag{10}$$

We have substituted $\rho_{\mathrm{S}_1}^{(3)} = Ae^{i\varphi_1}$, $\rho_{\mathrm{aS}_1}^{(3)} = Be^{i\varphi_2}$ from Eqs. (4) and (5) where A, B and φ_1,φ_2 are the moduli and phase angles of $\rho_{\mathrm{S}_1}^{(3)}$ and $\rho_{\mathrm{aS}_1}^{(3)}$, respectively. When Stokes and anti-Stokes signals propagate through the Pr:YSO crystal, a phenomenon of Kerr nonlinear phase shift results in cross-phase modulation (XPM). Based on the above Hamiltonian, the propagation dynamics is given as

$$da_{\mathrm{S}}/dt = \gamma_{\mathrm{S}}a_{\mathrm{S}} + \chi_S^{(3)}a_{\mathrm{aS}}^{+}\exp(i\varphi_{\mathrm{S}}), \tag{11}$$

$$da_{\mathrm{aS}}/dt = \gamma_{\mathrm{aS}}a_{\mathrm{aS}} + \chi_{\mathrm{aS}}^{(3)}a_{\mathrm{S}}^{+}\exp(i\varphi_{\mathrm{aS}}), \tag{12}$$

where φ is the induced nonlinear phase (φ_i) through XPM given by $\varphi_i = 2(k_i n_2^i |E_1|^2 e^{-r^2} z)/n_1$, n_1 is the linear refractive index, and $n_2^i = \mathrm{Re}\chi_i^{(3)}/\varepsilon_0 c n_1$ is the cross-Kerr nonlinear coefficient.

The second-order correlation function $G^{(2)}(\tau)$ between intensity fluctuations of two optical beams i, j, $i \neq j$, as a function of time delay τ is given by [20]

$$G_{ij}^{(2)}(\tau) = \frac{\langle\delta I_i(t)\delta I_j(t+\tau)\rangle}{\sqrt{\langle[\delta I_i(t)]^2\rangle\langle[\delta I_j(t+\tau)]^2\rangle}}. \tag{13}$$

The correlation function expressed using Eq. (13) may have pure sharp, pure broad, or a combination of sharp and broad peaks (two-stage shape). In two-mode correlation the shape of the correlation function for pure SPFWM (S-aS channel) is determined by [21]

$$A_{\text{S-aS}} = R_1|A_1|^2\{\exp(-2\Gamma_{\text{S-aS}}^{-}|\tau|) + \exp(-2\Gamma_{\text{S-aS}}^{-}|\tau|) - 2\cos(\Omega_e|\tau|)\exp[-(\Gamma_{\text{S-aS}}^{+} + \Gamma_{\text{S-aS}}^{-})|\tau|]\}, \tag{14}$$

and for the composite (FL+SPFWM) signal as

$$A_c = R_1|A_1|^2\{\exp[-2(\Gamma_{\text{S-aS}}^{+} + \Gamma_{\mathrm{FL}}^{+})|\tau|] + \exp[-2(\Gamma_{\text{S-aS}}^{-} + \Gamma_{\mathrm{FL}}^{-})|\tau|] - 2\cos(\Omega_e|\tau|)\exp[-(\Gamma_{\text{S-aS}}^{+} + \Gamma_{\mathrm{FL}}^{+} + \Gamma_{\text{S-aS}}^{-} + \Gamma_{\mathrm{FL}}^{-})|\tau|]\}. \tag{15}$$

The shape is primarily affected by the decay rate Γ. The degree of two-mode intensity-difference squeezing of signals i and j is given by [22]

$$Sq^{(2)} = \log_{10}\frac{\langle\delta^2(\hat{I}_i - \hat{I}_j)\rangle}{\langle\delta^2(\hat{I}_i + \hat{I}_j)\rangle}, \tag{16}$$

where $\langle\delta^2(\hat{I}_i - \hat{I}_j)\rangle$ is the mean square deviation of the intensity difference and $\langle\delta^2(\hat{I}_i + \hat{I}_j)\rangle$ is the mean square deviation of the intensity sum. For a medium with cross-Kerr effect, considering the relative nonlinear phase difference $\Delta\varphi$ between output Stokes and anti-Stokes signals, the intensity-difference squeezing function [Eq. (16)] can be calculated as

$$G_{\text{S-aS}}^{(2)}(\tau) = \frac{\langle\delta\hat{I}_{\mathrm{S}}(t_{\mathrm{S}})\delta\hat{I}_{\mathrm{aS}}(t_{\mathrm{aS}})\rangle}{\sqrt{\langle\delta\hat{I}_{\mathrm{S}}(t_{\mathrm{S}})^2\rangle\langle\delta\hat{I}_{\mathrm{aS}}(t_{\mathrm{aS}})^2\rangle}}\cos(\Delta\varphi), \tag{17}$$

$$Sq^{(2)} = \log_{10}\left[\frac{\langle\delta^2(\hat{I}_{\mathrm{S}} - \hat{I}_{\mathrm{aS}})\rangle}{\langle\delta^2(\hat{I}_{\mathrm{S}} + \hat{I}_{\mathrm{aS}})\rangle}\right]\cos(\Delta\varphi). \tag{18}$$

The output field is not a free field as it is generated by a nonlinear crystal (source). Hence the source field does not hold a commutation relation because the commutation is an incorrect physical description of a quantum mechanical filtered field [4]. The field transmitted by the filter used in the detector uses a timely order frequency filtered autocorrelation function [5], which contains no commutation terms [4]. However, in quantum optics the normal time-ordered product appears, which can describe the commutation relation.

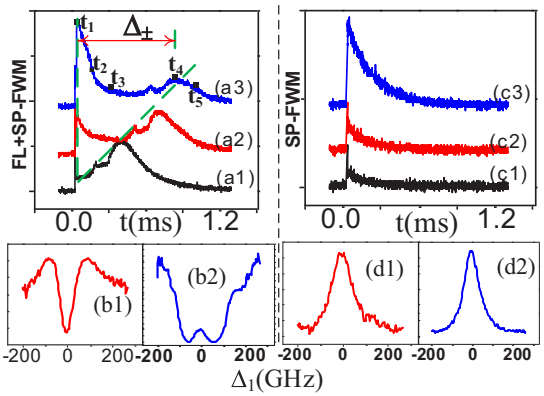

FIG. 2. In two-level atomic system (a1)–(a3) show the evolution of the intensity of the composite (FL+SPFWM) signal in time domain as power increases. (b1),(b2) show the spectral domain signals of (a2),(a3), respectively. (c1)–(c3) show the intensity of a pure SPFWM signal in time domain as power increases. (d1),(d2) show the spectral domain signals of (c2),(c3), respectively. The power of $E_1(P_1)$ changes from medium (8 mW) to high (9 mW) and to very high power (10 mW) while the power of $E_2(P_2)$ is fixed.

The generalized extension of Eq. (13) for the three-mode correlation function, $G^{(3)}(\tau_i,\tau_j,\tau_k)$, is given as

$$G^{(3)}(\tau_i,\tau_j,\tau_k)=\frac{\langle[\delta\hat{I}_i(\tau_i)][\delta\hat{I}_j(\tau_j)][\delta\hat{I}_k(\tau_k)]\rangle}{\sqrt{\langle[\delta\hat{I}_i(\tau_i)]^2\rangle\langle[\delta\hat{I}_j(\tau_j)]^2\rangle\langle[\delta\hat{I}_k(\tau_k)]^2\rangle}}, \quad (19)$$

where $i,j,k=1,2,3; i\neq j\neq k$). The shape of the three-mode correlation function is determined as

$$A = B\int d\omega_2\left|e^{-i\omega_2\tau_3}\frac{\kappa_1\kappa_2\sinh^2(\Omega L)\cosh(\Omega t)}{\Omega^2}\right|^2 - C\int d\omega_2\left[e^{-i\omega_2(\tau_2-\tau_1)}\frac{\kappa_1\sinh(\Omega L)\cosh(\Omega L)}{\Omega}\right], \quad (20)$$

where B and C are parameters that affect the magnitude of correlation. Ω is the Rabi frequency, L is the length of the medium, and κ is the nonlinear coefficient. The function in Eq. (20) is related to τ and as a result determines the shape of the three-mode correlation function $G^{(3)}(\tau_1,\tau_2,\tau_3)$. In the three-mode case, the corresponding intensity-difference squeezing defined in Eq. (16) can be given by [23]

$$Sq^{(3)}=\log_{10}\frac{\langle\delta^2(\hat{I}_i-\hat{I}_j-\hat{I}_k)\rangle}{\langle\delta^2(\hat{I}_i+\hat{I}_j+\hat{I}_k)\rangle}, \quad (21)$$

where $\langle\delta^2(\hat{I}_i+\hat{I}_j+\hat{I}_k)\rangle=\langle(\hat{I}_i+\hat{I}_j+\hat{I}_k)^2\rangle-\langle\hat{I}_i+\hat{I}_j+\hat{I}_k\rangle^2$ and $\delta^2(\hat{I}_i-\hat{I}_j-\hat{I}_k)=\langle(\hat{I}_i-\hat{I}_j-\hat{I}_k)^2\rangle-\langle\hat{I}_i-\hat{I}_j-\hat{I}_k\rangle^2$.

IV. EXPERIMENTAL RESULTS AND DISCUSSION

The time domain intensity evolution of a SPFWM+FL composite signal and a pure SPFWM signal are shown in Figs. 2(a1)–2(a3) and 2(c1)–2(c3), respectively. The power of P_1 changed from medium (8 mW) to high (9 mW) and then to very high power (10 mW) in Figs. 2(a1)–2(a3) and 2(c1)–2(c3). Figures 2(b1), 2(b2), 2(d1), and 2(d2) show the corresponding spectral signal intensities of Figs. 2(a2), 2(a3), 2(c2), and 2(c3), respectively. Figures 2(a1)–2(a3) show Autler-Townes (AT) splitting in a fourth-order FL composite signal due to the dressing effect of E_1 with increasing splitting distance from left to right peaks with increased power as indicated by the oblique dashed line across Figs. 2(a1)–2(a3). With such time position differences at larger powers, we can neglect interference effects. Figures 2(b1) and 2(b2) show the suppression dip of FL at $\Delta_1=\Delta_2=0$ and the emergence of a small emission peak of impure SPFWM (Stokes), respectively. The emission peak [Fig. 2(b2)] of SPFWM evolves out of the suppression dip of the FL signal, which shows the existence of competition between FL and SPFWM.

This phenomenon is consistent with the self-dressing effect of field $\mathbf{E}_1(G_1|^2/d_1)$ as predicted in Eq. (3). To explain further, the total intensity of the composite signals (SPFWM+FL) can be written as $\rho=\rho^{(4)}_{\rm FL}+\rho^{(3)}_{\rm SPFWM}$, where $\rho^{(3)}_{\rm SPFWM}=\rho^{(3)}_{\rm S_2}$ or $\rho^{(3)}_{\rm SPFWM}=\rho^{(3)}_{\rm aS_2}$. Due to a dressing-induced completion effect the delay time between the composite signals increases with power as shown in Figs. 2(a1)–2(a3). This is explained as adiabatic residual particle transfer from $|G_{1+}\rangle$ to $|G_{1-}\rangle$ through phonon-assisted nonradiative transition which is mainly determined by acoustic phonons at low temperature [12]. In the left peak of the composite signal (along t_1 to t_2) the intensity term of SPFWM ($\rho^{(3)}_{\rm SPFWM}$) increases linearly due to the gain effect of the generating field E_1 as predicted by Eqs. (1) and (2). The same effect is observed in pure SPFWM in which the signal intensity is highly enhanced at very high power as shown in Figs. 2(c1)–2(c3). The smooth curve (less noise) in the spectral domain in Fig. 2(d2) agrees with the enhancement of SPFWM at increased power. However, in the composite signal, the term $\rho^{(4)}_{\rm FL}$ first increases with $|G_1|^2$ and gradually decreases due to the dressing effects of $|G_1|^2/\Gamma_{00}$ and $|G_1|^2/d_1$ in Eq. (3) as we can observe in Figs. 2(a1)–2(a3). The right peaks at time positions t_4 and t_5 correspond to FL signals. The intensity of the measured multipeak FL signal is expressed using Eq. (8). These two FL peaks at t_4 and t_5 correspond to the dressed states $|G_{1+}\rangle$ and $|G_{1-}\rangle$, which indicates that the FL signal is more sensitive for dressing than SPFWM [14] as shown in Fig. 2(a3). Consequently, at very high power, FL intensity is suppressed and SPFWM intensity is enhanced as shown in Fig. 2(a3). To further investigate, we set $|1\rangle$ as the frequency reference point and the Hamiltonian can be written as $H=-\hbar[\begin{smallmatrix}0 & G_1\\ G_1^* & (-1)^i\Delta_1\end{smallmatrix}]$. From the equation $H|G_{1\pm}\rangle=\lambda_\pm|G_{1\pm}\rangle$, we can obtain the eigenvalues $\lambda_\pm=[(-1)^i\Delta_1\pm\sqrt{\Delta_1^2+4|G_1|^2}]/2$. The splitting distance $\Delta_\pm=\lambda_+-\lambda_-$ between $|G_{1+}\rangle$ and $|G_{1-}\rangle$ is given as $\Delta_\pm=\lambda_+-\lambda_-=\sqrt{\Delta_1^2+4|G_1|^2}$, where $G_1=\mu(2P_1/\varepsilon_o cA)^{1/2}/\hbar$. Thus, with P_1 increasing, the splitting distance increases due to the term $(|G_1|^2)$ as shown in Fig. 2(a).

A. Two-mode correlation and squeezing

Figure 3 shows correlation and squeezing of SPFWM and FL signals for selected time positions in the time delay curve in Fig. 2(a) in a two-level system. First intensity fluctuations $\delta I_{\rm S\text{-}aS}$ and $\delta I_{\rm FL}(t+\tau)$ are measured at each selected time

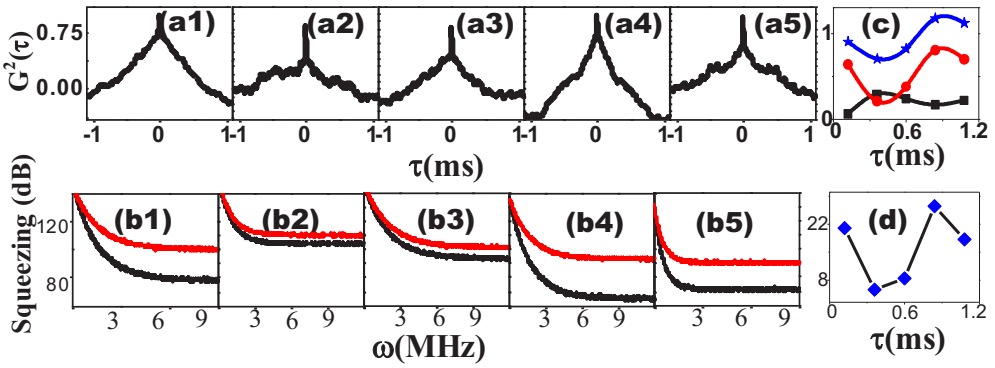

FIG. 3. (a1)–(a5) show two-mode intensity-noise correlation of composite signal (FL+SPFWM) at different selected time positions for a two-level system as shown in Fig. 2(a). (b1)–(b5) show the corresponding intensity-difference squeezing. (c) shows the correlation amplitude dependence of (a1)–(a5). The broad, sharp, and total amplitude dependences are shown by the circle connector curve (middle curve in red), square connector curve (lower curve in black), and star connector curve (upper curve in blue), respectively. (d) shows total squeezing dependence of (b1)–(b5).

position and plotted as a function of time delay (τ) using (i = S-aS, j = FL) from Eq. (13).

Correlation curves in Figs. 3(a1)–3(a5) and the corresponding squeezing curves in Figs. 3(b1)–3(b5) are for different time positions t_1–t_5 labeled in Fig. 2(a). The sharp peak, broad peak, and total amplitude dependence of correlation values at $\tau = 0$ for Figs. 3(a1)–3(a5) are shown in Fig. 3(a6) as square, circle, and star connector curves, respectively. The role of such lines is consistent for the remaining figures described subsequently. The corresponding magnitude of squeezing is shown in the trend line shown in Fig. 3(b6). We observe that the magnitude of correlation follows the intensity of the composite signal and the competition between SPFWM and FL signals as shown in Fig. 2(a). The black and the red lines represent the intensity-difference signal $\delta^2(\hat{I}_i - \hat{I}_j)$ and the noise signal $\delta^2(\hat{I}_i + \hat{I}_j)$, respectively. The competition between SPFWM and FL composite signals determines the two-stage shape of the correlation function [Figs. 3(a1)–3(a5)] given by Eq. (15) which is determined by the decay rate Γ of the signals involved. Due to the interaction of coupling fields, the homogeneous linewidth broadening of the measured fluorescence signal is given as $\Gamma_{\text{pop}} + \Gamma_{\text{ion-spin}} + \Gamma_{\text{ion-ion}} + \Gamma_{\text{phonon}}$ [19], where $\Gamma_{\text{pop}} = (2\pi T_1)_1^{-1}$ is the population decay time which depends on the location of the energy level in phase space, $\Gamma_{\text{ion-spin}}$ is the ion-spin coupling effect of the individual ion, $\Gamma_{\text{ion-ion}}$ is due to the ion-ion interaction among the rare-earth ions, and Γ_{phonon} is decay related to the thermal effect. The last three terms are components of $(2\pi T_2^*)_1^{-1}$ [the dephasing or coherence time T_2^*)]. The linewidth of the coherence process of a two-level system between two energy levels $|i\rangle$ and $|j\rangle$ can be described as $\Gamma_{ij} = (\Gamma_i + \Gamma_j)/2, (i, j = 0, 1, \cdots)$. We can express the population decay time (T_1) and the coherence time (T_2^*) by setting the relation $(\Gamma_m)_n = (2\pi T_1)_{mn}^{-1} + (2\pi T_2^*)_{mn}^{-1}$, where m is the level state and n is the order of perturbation chain in the density matrix. The intensity of the measured fluorescence signal in two levels is $I_{\text{FL}}(t) = \rho_{\text{FL}}^{(4)} \exp(-\Gamma_{\text{FL}} t)$, where $\Gamma_{\text{FL}} = \Gamma_{11} + \Gamma_{10}$ in which $\Gamma_{10} = (2\pi T_1)_1^{-1}$ is the transverse dephasing rate of ground state $|0\rangle$. Considering the controlling terms we can write $(2\pi T_1)_1^{-1} = 6\pi(\upsilon + \Delta\upsilon)^3 \beta^2 \eta^3 / \varepsilon h c^3$, $(2\pi T_1)_0^{-1} = 0$, $(2\pi T_2^*)_1^{-1} = P_1(t) + \gamma_0$, $(2\pi T_2^*)_0^{-1} = P_0(t) + \gamma_0$, where γ_0 is the total effect of Γ_{phonon} and $\Gamma_{\text{ion-spin}}$, and

$$P_0(t) = \exp\left[-c_H \sum_{\substack{n=6,8,10,\\ 12,13,14}} \left(A_{nH}/R_H^n\right)\right], \tag{22}$$

$$P_1(t) = \exp\left[-c_D \sum_{n=5,6,7} \left(A_{nD}/R_D^n\right)\right]. \tag{23}$$

The term $(\upsilon + \Delta\upsilon)$ represents the dressed state location of the energy level. c_H and c_D represent the population densities at the triplet energy level $^3H_4$ and singlet energy level $^1D_2$, respectively, controlled by the pump power. $\sum (A_{nH}/R_H^n)$ and $\sum (A_{nD}/R_D^n)$ are the induced dipole-dipole interactions of states H-H and D-D, respectively. Similarly for the SPFWM signals (E_{S} and $E_{a\text{S}}$) we can describe them as $I_{\text{S}_2}(t) = I_{0(\text{S}_2)} \exp(-\Gamma_{\text{S}_2} t)$, $I_{\text{aS}_2}(t) = I_{0(\text{aS}_2)} \exp(-\Gamma_{\text{aS}_2} t)$, where $I_{0(\text{S}_2)} \propto |\rho_{10(\text{S}_2)}^{(3)}|^2$ and $I_{0(\text{aS}_2)} \propto |\rho_{10(\text{aS}_2)}^{(3)}|^2$, and $\Gamma_{\text{S}}^{\pm} = \Gamma_{\text{aS}}^{\pm} = 2\Gamma_{10} + \Gamma_{00}$. For the total composite signal in a two-level system, $\Gamma^{\pm} = \Gamma_1 + \Gamma_2 = 4\Gamma_{10} + 3\Gamma_{00}$. The shape of the correlation function for the SPFWM and FL composite signals is given by

$$\begin{aligned} A_c = {} & R_1 |A_1|^2 \{\exp[-2(\Gamma_1^+ + \Gamma_2^+ + \zeta)|\tau|] \\ & + \exp[-2(\Gamma_1^- + \Gamma_2^- + \zeta)(|\tau|)]\} \\ & - 2\cos(\Omega_e|\tau|)\exp[-(\Gamma_1^+ + \Gamma_2^+ + \Gamma_1^- + \Gamma_2^- + \zeta)|\tau|], \end{aligned}$$

where $\Gamma_1 = \Gamma_{\text{S-aS}}$ and $\Gamma_2 = \Gamma_{\text{FL}}$. The parameter ζ represents the bandwidth of the source laser and is constant. Thus the broadness and sharpness of the correlation peaks are determined by decay rate Γ. Unlike FL signals, SPFWM signals are generated via coherent processes whose linewidths are determined by atomic coherence time and are thus much narrower. Thus SPFWM decays faster (larger Γ) than the FL signal (smaller Γ) corresponding to broad to sharp peak transition with decreasing power as shown in Fig. 3(a). With similar argument, the magnitude of intensity-difference squeezing in Figs. 3(b1)–3(b5), which is described as the

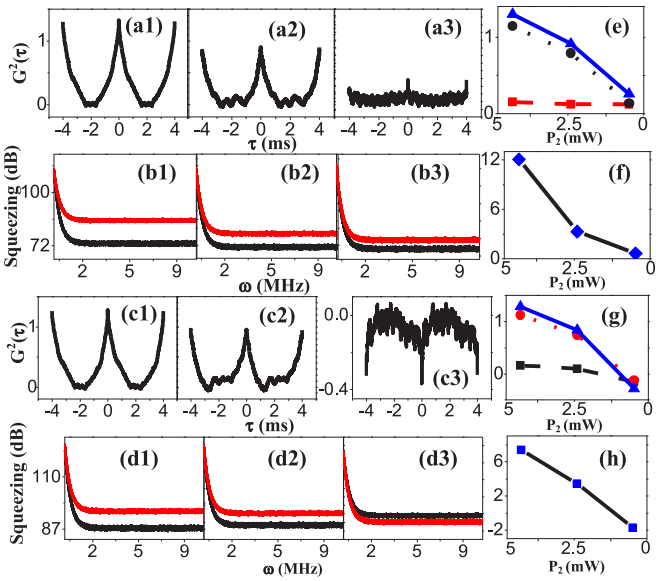

FIG. 4. (a1)–(a3) show two-mode intensity-noise correlation and intensity-difference squeezing of Stokes and anti-Stokes SPFWM from PMT1 and PMT2; (c1)–(c3) Stokes–anti-Stokes and fourth-order FL from PMT1 and PMT3 in two-level system by changing power of E_1 from high (left) to low (right) from 5 to 0 mW while P_2 is kept constant. (b1)–(b3) and (d1)–(d3) show the corresponding two-mode squeezing. (e),(g) show the trend of corresponding broad peak (red dotted line curve), sharp peak (black dash line curve), and total correlation amplitude (blue curve). (f),(h) show the corresponding magnitude of squeezing.

gap between the black and red curves as shown in Fig. 3(d), changes comparably with total correlation values in Fig. 3(c).

Figure 4 shows two-mode correlation and squeezing of Stokes–anti-Stokes and FL composite signals when power decreases from high (left) to low (right). The SPFWM (E_S and E_{aS}) are generated by opening both $E_1(\Delta_1,\omega_1)$ and $E_2(\Delta_2,\omega_2)$ fields satisfying the phase-matching condition $\mathbf{k_1}+\mathbf{k_2}=\mathbf{k_{S1}}+\mathbf{k_{aS1}}$. The generated twin photons propagate in the opposite directions and are reflected by the PBS and are detected by PMT1 and PMT2 as shown in Fig. 1(b). The FL signal generated accompanying SPFWM is detected by PMT3 [Fig. 1(b)]. Two-mode correlation and squeezing of S+aS and S-aS+FL composite signals are shown in Figs. 4(a)–4(d), respectively. The correlation function of the Stokes and anti-Stokes pair is calculated by time-dependent intensity fluctuation described by Eq. (13). The intensity fluctuations $d\hat{I}_S(t_S)d\hat{I}_{aS}(t_{aS})$ are recoded and plotted as shown in Fig. 4(a). Figures 4(a1)–4(a3) shows that the total correlation peak values of pure SPFWM decrease as power decreases. A maximum correlation value of 1.3 is obtained as given in Fig. 4(a1). The corresponding measured squeezing values also decrease as clearly shown in the total squeezing trend in Fig. 4(f). Similarly, the trend of both total correlation and squeezing values as power decreases is shown in Figs. 4(g) and 4(h), respectively. A squeezing value of -1.75 dB was measured for SPFWM+FL composite signals as shown in Fig. 4(d3). The result is explained by the total phase difference between the composite signals induced by SPM due to the dressing effect of field $E_1[|G_1|^2/(\Gamma_{00}+i(\Delta_2-\Delta_1)$ and $|G_1|^2/\Gamma_{00}]$ in Eqs. (1) and (2) and initial phase induced by XPM. From the evolution of SPFWM and FL signals, as power changes one can determine the total phase characteristics $\Delta\varphi_T=\Delta\varphi_I+\Delta\varphi_N$ of the composite signal by considering the phase of output Stokes and anti-Stokes $\Delta\varphi_N$, and initial phase $\Delta\varphi_I=\varphi_{FL}-\varphi_{aS}$ due to the signals' source difference. For pure SPFWM in Figs. 4(a) and 4(b), the total phase is determined by $\Delta\varphi_N$ between Stokes and anti-Stokes signals $\Delta\varphi_T=\Delta\varphi_N=2(k_S n_2^S-k_{aS}n_2^{aS})|E_1|^2e^{-r^2}z/n_1$ induced by SPM. With the nonlinear phase change, the intensity-noise correlation function $G^{(2)}_{\text{S-aS}}(\tau)$ between Stokes and anti-Stokes signals can be calculated by Eq. (17). The corresponding intensity-difference squeezing associated with relative nonlinear phase is obtained using Eq. (18). When the power of P_1 is set to change from 5 to 1 mW, the corresponding nonlinear phase change due to SPM is from $\Delta\varphi=0$ to $\Delta\varphi=\pi/4$. However, for the composite signal in Figs. 4(c) and 4(d) the total phase $\Delta\varphi_T$ is affected by both nonlinear phase change $\Delta\varphi_N$ and the initial phase change $\Delta\varphi_I$. The magnitude of total phase change $\Delta\varphi_T=\Delta\varphi_I+\Delta\varphi_N$ is determined by the nature of the composite signals involved. For the composite signal, the phase difference is larger due to the incoherent nature of the FL signal as compared to the coherent S-aS signals. When the power of P_1 changes from 5 to 1 mW, the corresponding total phase $\Delta\varphi_T=\Delta\varphi_I+\Delta\varphi_N$ changes from $\Delta\varphi=0$ to $\Delta\varphi=\pi$. Specifically, at $\Delta\varphi_T=\pi$, we observe anticorrelation and antisqueezing in Figs. 4(c3) and 4(d3), respectively. Figures 4(b1), 4(b3), 4(d1), and 4(d3) show that the magnitude of intensity-difference squeezing decreases with power change in the same way as correlation decreases.

Now let us focus on the shape of correlation curves in Fig. 4. For a pure S+aS signal, we observe from Fig. 2(c) that the signal intensity increases with power leading to decrease in decay rate $\Gamma^{\pm}=2\Gamma_{10}+\Gamma_{00}$. The shape of the correlation function for pure SPFWM as a function of decay rate Γ is given by

$$\begin{aligned}A_{\text{S}_2\text{-aS}_2}=R_1|A_1|^2\{&\exp[-(2\Gamma^-+\zeta)|\tau|]\\&+\exp[-(2\Gamma^-+\zeta)|\tau|].\\&-2\cos(\Omega_e|\tau|)\exp[-(\Gamma^++\Gamma^-+\zeta)|\tau|]\},\end{aligned}$$

where $\Gamma^{\pm}=\Gamma_{\text{S}_2\text{-aS}_2}$. Thus as power decreases the shape of the correlation function changes from a broad to a sharp peak as shown in Fig. 4(a). Similarly, the shape of the correlation function for composite (SPFWM+FL) signals shown in Fig. 4(c) is given by

$$\begin{aligned}A_c=R_1|A_1|^2\{&\exp[-2(\Gamma_1^++\Gamma_2^++\zeta)|\tau|]\\&+\exp[-2(\Gamma_1^-+\Gamma_2^-+\zeta)|\tau|].\\&-2\cos(\Omega_e|\tau|)\exp[-(\Gamma_1^++\Gamma_2^++\Gamma_1^-+\Gamma_2^-+\zeta)|\tau|]\},\end{aligned}$$

where $\Gamma_1^{\pm}=\Gamma^{\pm}_{\text{S}_2\text{-aS}_2}$ and $\Gamma_2=\Gamma_{\text{FL}}$. The total decay rate is $\Gamma_1^{\pm}+\Gamma_2^{\pm}=\Gamma_{\text{S}_2\text{-aS}_2}+\Gamma_{\text{FL}}$ where $\Gamma_{\text{S}_2\text{-aS}_2}=2\Gamma_{10}+\Gamma_{00}$, $\Gamma_{\text{FL}}=2(\Gamma_{00}+\Gamma_{10})$. Therefore, the total decay rate of the composite signal is $\Gamma=4\Gamma_{10}+3\Gamma_{00}$. That is, the SPFWM signal has a faster decay rate than the FL signal. As discussed in Fig. 3, the linewidth of SPFWM is narrower than that of the FL signal due to its coherence property, which agrees with the broad to sharp peak transition we observe in Figs. 4(a) and

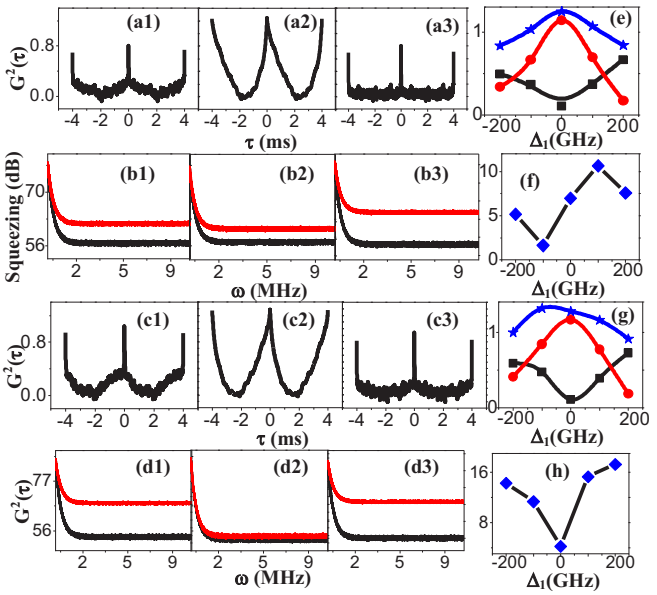

FIG. 5. (a1)–(a3) show two-mode intensity-noise correlation and intensity-difference squeezing of Stokes and anti-Stokes SPFWM from PMT1 and PMT2; (c1)–(c3) Stokes–anti-Stokes and fourth-order FL from PMT1 and PMT3 in three-level V-type system by scanning detuning Δ_1 from –200 to + 200 GHz and setting $\Delta_2 = 0$. (b1)–(b3) and (d1)–(d3) show the corresponding two-mode squeezing. (e),(g) show the trend of corresponding broad peak (middle circle connector curve in red), sharp peak (lower square connector curve in black), and total correlation amplitude (upper star connector curve in blue) for (a1)–(a3) and (c1)–(c3), respectively. (f),(h) show the corresponding magnitude of squeezing for (b1)–(b3) and (d1)–(d3), respectively.

4(c). Thus the broad peak amplitude decreases with power as seen from Fig. 4(e). Similarly, in the composite SPFWM+FL signal, since SPFWM dominates at larger power and FL signal dominates at low power, there is a broad to sharp peak transition as power decreases as depicted in Fig. 4(g).

Finally, in Fig. 5 we present the dependence of three-mode intensity-noise correlation and squeezing on frequency detuning (Δ_1). The intensities of the Stokes, anti-Stokes, and the fourth-order FL signals are obtained by scanning Δ_1 from -200 to 200 GHz and keeping $\Delta_2 = 0$. The intensity-noise traces $\delta\hat{I}_S(t_S)$ and $\delta\hat{I}_{aS}(t_{aS})$ are measured and two- and three-mode intensity-noise correlation and intensity-difference squeezing versus τ are plotted using Eqs. (14)–(18) as shown in Figs. 5 and 7, respectively. We first investigate the intensity-noise correlation between Stokes, anti-Stokes, and FL signals in the V-type three-level system. Figures 5(a1), 5(a3), 5(c1), and 5(c3) show two-mode intensity-noise correlation versus τ at different detunings of Δ_1 between the S+aS and the SPFWM+FL composite signal, respectively. The corresponding two-mode intensity-difference squeezing is shown in Figs. 5(b1), 5(b3), 5(d1), and 5(d3), respectively.

It is found that in both pure SPFWM and the composite signal, correlation attains a maximum value at resonance ($\Delta_1 = 0$) and decreases at off resonance ($|\Delta_1| > 0$). This is explained as dressing-induced modulation of $\chi^{(3)}_{\text{S-aS}}$ of Eqs. (4) and (5). When Δ_1 is tuned near the resonance (0 GHz), the higher-order nonlinear process becomes stronger and increases the nonlinear gain due to nonlinear susceptibility κ overcoming the dominance of the SPFWM process; hence the correlation is increased. The gain of Stokes and anti-Stokes signal expressed in Eqs. (9) and (10) determined by nonlinear susceptibility $\chi^{(3)}_{S_1,aS_1} = (N\mu_{S,aS}\rho^{(3)}_{S_1,aS_1})/(\varepsilon_0 E_1 E_2 E_{S_1,aS_1})$ for the V-type system is shown in Fig. 1(a) and the intensity is proportional to photon number $[I_i(t_i) = N_i \exp(-\Gamma_i t_i)$ $(i = S_1, aS_1)]$. $G^{(2)}(\tau)$ depends on the nonlinear susceptibility $\chi^{(3)}_{Si,aSi}$ which is expressed in terms of density-matrix elements in Eqs. (4) and (5). $\chi^{(3)}_{Si,aSi}$ is determined by the dressing terms in Eqs. (4) and (5). The intensity of the composite signal is determined by the dressing terms in Eqs. (6) and (7).

The shape of such correlation function is determined by Eq. (14). For pure SPFWM the total decay rate can be written as $\Gamma = \Gamma_{S_1} + \Gamma_{aS_1} = 2(\Gamma_{00} + \Gamma_{10} + \Gamma_{20})$. The value of decoherence rate Γ decreases with decreasing detuning Δ_1, and attains a minimum value at $\Delta_1 = 0$ due to strong interaction among ions as a result of the dressing effect [14]. Thus smaller Γ at resonance corresponds to broad peak correlation and longer Γ at off resonance corresponds to sharp peak correlation. Similarly, for the composite signal the total decay rate is given as $\Gamma = \Gamma_{S_1-aS_1} + \Gamma_{FL_1} + \Gamma_{FL_2}$, where $\Gamma_{S_1} = \Gamma_{aS_1} = \Gamma_{20} + \Gamma_{00} + \Gamma_{10}$. In both pure SPFWM [Figs. 5(a) and 5(b)] and composite signals [Figs. 5(c) and 5(d)], correlation and squeezing attain a maximum at resonance and off resonance, respectively. This can be explained as the enhancement and suppression of the signal intensity due to bright and dark states induced by the dressing effect of the field E_1 [13]. When we compare squeezing at resonance in Figs. 5(b) and 5(d) we observe that the squeezing for pure SPFWM (S-aS channel) shown in Fig. 5(b) is larger than that of the SPFWM and FL composite signals shown in Fig. 5(d). This is due to the FL signal mixture which has a larger linewidth and thus more classical noise. That is, in Fig. 5(d) at off resonances the intensity-noise sum (red curve) rises higher than at resonance, which is attributed to noise from the FL signal. The nonclassicality of generated photons depends on which component of the composite signals is dominant and can be proved by checking whether the correlation between the photon pairs violates the inequality or not from the experimental result. Classical lights satisfy the Cauchy-Schwarz inequality $R = g^{(2)}_{S_1,S_2}(\tau)/g_{S_1,S_1}g_{S_2,S_2} \leqslant 1$ [16], where g_{S_1,S_1} and g_{S_2,S_2} are autocorrelations and $g^{(2)}_{S_1,S_2}(\tau)$ is cross-correlation between signal 1 and signal 2. In the SPFWM+FL composite signal, a total correlation value of $R = 1.4 > 1$ is obtained at resonance, which clearly demonstrates the violation of the Cauchy-Schwarz inequality as shown in the amplitude dependence curves in Figs. 5(e) and 5(g). Thus it proves that the correlation is a nonclassical effect, owing to the dominance of SPFWM at resonance where the coupled fields are used to reduce noise. Comparing the two-level system with the three-level V-type atomic systems, larger correlation and squeezing are obtained in the two-level atomic system.

B. Three-mode correlation and squeezing

In this section we continue to investigate the shape of hybrid three-mode correlation and the magnitude of squeezing

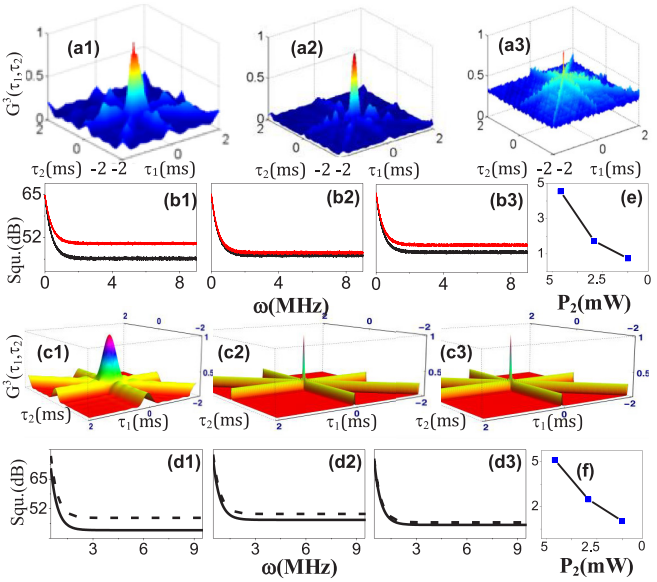

FIG. 6. (a1)–(a3) and (b1)–(b3) show the experimental result of three-mode correlation $G^3(\tau_1,\tau_2,\tau_3)$ versus time delay (τ_1,τ_2,τ_3) and squeezing for same experiment conditions as in Figs. 4(c1)–4(c3) and 4(d1)–4(d3) for SPFWM+FL composite signal. (c1)–(c3) and (d1)–(d3) show the simulated theoretical prediction of three-mode correlation and squeezing. In (d1)–(d3) the solid and dashed lines show the intensity-difference and intensity-noise sum signals, respectively. The trends of squeezing for experimental and theoretical simulation results are shown in (e),(f), respectively.

through the dressing-induced competition effect. In this case, all three signals (Stokes, anti-Stokes, and FL) are taken by opening both pumping fields E_1 and E_2 simultaneously. Since the same sample was used, both two and three modes share the pumping field E_1 and the dressing field E_2 through nonlinear gain $g = |(-i\omega_{S,aS}\chi^{(3)}_{S,aS}E_1E_2)/2c|$and FL signal intensity $\rho^{(4)}_{FL}$. Thus three-mode correlation and squeezing are related to nonlinear gain which is in turn determined by the nonlinear susceptibility $\chi^{(3)}_{S,aS} = (N\mu_{S,aS}\rho^{(3)}_{S,aS})/(\varepsilon_0 E_1E_2E_{S,aS})$ and FL intensity.

Figures 6(a1)–6(a3) and 6(b1)–6(b3) show the experimental results of three-mode correlation and squeezing for the same experimental conditions as in Fig. 4 for the SPFWM+FL composite signal in a V-type atomic system. In a V-type system the total intensity of the composite signal is $\rho = \rho_{FL} + \rho_{SPFWM}$ where $\rho_{FL} = \rho^{(4)}_{FL_1} + \rho^{(4)}_{FL_2}$ and $\rho_{SPFWM} = \rho^{(3)}_{S_1}$ or $\rho^{(3)}_{aS_1}$. The intensity fluctuations $\delta\hat{I}_1(\tau_1)$, $\delta\hat{I}_2(\tau_2)$, and $\delta\hat{I}_3(\tau_3)$ are recorded and the triple beam $(S + aS + FL)$ intensity-noise correlation is plotted using Eq. (19). Similarly, the three-mode intensity-difference squeezing is plotted using Eq. (21) for the triple beams. Figures 6(c1)–6(c3) and 6(d1)–6(d3) show the simulated theoretical predictions of hybrid three-mode correlation and squeezing, which are comparable with the experimental results obtained. In Figs. 6(d1)–6(d3) the solid and dashed lines show the intensity-difference and intensity-noise sum signals, respectively. The shape of the correlation curves in Figs. 6(a1)–6(a3) and 6(b1)–6(b3) is governed by Eq. (20) in a similar way as in Eqs. (14) and (15) for two-mode correlation. The decay rate Γ of the composite signal is determined by the combined effect of both the

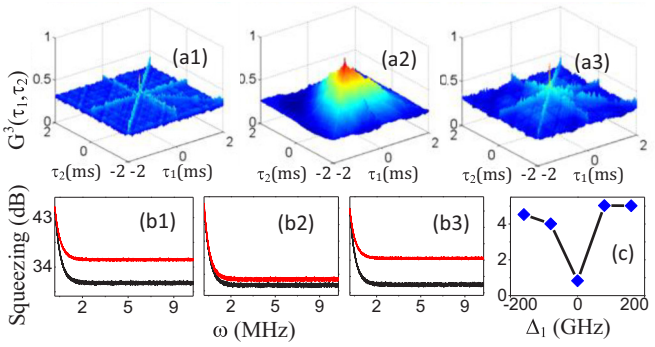

FIG. 7. Three-mode intensity-noise correlation $G^3(\tau_1,\tau_2)$ versus delay time (τ_1,τ_2) and intensity-difference squeezing of Stokes, anti-Stokes, and fourth-order FL in three-level (V-type system) by scanning detuning Δ_1 from –200 to +200 GHz and setting $\Delta_2 = 0$. (b1)–(b3) show the corresponding three-mode squeezing. (c) shows the trend of magnitude of squeezing at resonance and off resonance.

source difference between the signals and the competitive dominance effect of the SPFWM and FL signals which dominate at high and low power, respectively. Total decay rate of the composite signal can be written as $\Gamma = \Gamma_{S_1} + \Gamma_{aS_1} + \Gamma_{FL_1} + \Gamma_{FL_2}$, where $\Gamma_{S_1} = \Gamma_{aS_1} = \Gamma_{00} + \Gamma_{10} + \Gamma_{20}$, $\Gamma_{FL_1} = \Gamma_{20} + \Gamma_{00} + \Gamma_{10} + \Gamma_{11}$, and $\Gamma_{FL_2} = \Gamma_{10} + \Gamma_{00} + \Gamma_{20} + \Gamma_{22}$. The decay rate Γ increases as power decreases which gives rise to the change in shape of correlation determined by Eq. (20) to change from broad to sharp as power decreases. The result agrees with that of two-mode correlation described in Fig. 4. Figures 6(b4) and 6(d4) show the trend of squeezing as power decreases for the experimental result and theoretical predictions, respectively. However, due to the signals' source difference the hybrid three-mode correlation and squeezing fails to show the anticorrelation and antisqueezing obtained in two-mode correlation shown in Figs. 4(c3) and 6(d3).

In Fig. 7 we further explain the dressing-induced competition effect between the composite signals which in turn affect the shape of hybrid three-mode correlation and magnitude of squeezing due to frequency detuning change. Figures 7(a1)–7(a3) and 7(b1)–7(b3) show the three-mode counterpart of correlation and squeezing for the same experiment condition as in Figs. 5(c1)–5(c3) and 5(d1)–5(d3), respectively. Signals from PMT1, PMT2, and PMT3 [Fig. 1(b)] are simultaneously considered in three-mode correlation. The competition effect is demonstrated in Figs. 7(a1)–7(a3) and 7(b1)–7(b3). Due to increased dressing effect of field $E_2(|G_2|^2/\Gamma_{00}, |G_2|^2/d_{21}$, and $|G_2|^2/d_2)$ at resonance in Eqs. (4)–(7) on both S-aS and FL channels, the dressing-induced dark state increases and the decay rate Γ gets smaller than the values at off resonance. Thus the shape of the hybrid intensity-noise correlation determined by Eq. (20) gets broader at resonance. The result obtained in Figs. 7(a) and 7(b) is comparably consistent with the results obtained in the two-mode case under Fig. 5, where the highest correlation is obtained at resonance and the largest classical squeezing (with FL noise) is obtained at off resonances.

V. CONCLUSION

Two-mode and three-mode correlation and intensity-difference squeezing of composite SPFWM and FL

signals controlled by changing power and detuning have been comprehensively analyzed in two-level and V-type three-level atomic systems based on the SPFWM process in a $Pr^{3+}:Y_2SiO_5$ crystal. It is found out that the dressing-induced competition effect between SPFWM and FL signals determines the two-stage shape of correlation and magnitude of squeezing. In addition, the results show that correlation and squeezing change to anticorrelation and antisqueezing, respectively, when power decreases. The effect is explained by induced cross-phase modulation due to the dressing field. A larger magnitude of correlation and squeezing is observed at high power which varies with power change proportionally. However, in frequency detuning change, a larger magnitude of correlation and squeezing is observed at resonance and off resonance, respectively. The larger magnitude of classical squeezing observed at off resonance is attributed to rising of intensity-noise sum level due to the FL mixture. Furthermore, a total correlation value of $R = 1.4 > 1$ is measured at resonance where the SPFWM signal dominates, indicating a violation of the Cauchy-Schwarz inequality. Correlation properties of coupled fields can be used to reduce the noise level. Such progress may find potential application in optical hybrid communication and information processing.

ACKNOWLEDGMENTS

We acknowledge financial support from the National Basic Research Program of China (2012CB921804), the National Natural Science Foundation of China (Grants No. 11474228 and No. 61205112), and Key Scientific and Technological Innovation Team of Shaanxi Province (2014KCT-10).

APPENDIX: DRESSING PERTURBATION

Here we will derive the steady-state density-matrix elements for the SPFWM and FL signals using the semiclassical picture of laser radiation. The steady-state density-matrix elements for the different setups were derived using Liouville or von Neumann equations. We have adopted the perturbation theory to obtain the Stokes and anti-Stokes signals under the weak-field condition (weak-field approximation). Then, the dressing terms of the strong pump field are incorporated. That is, we have adopted the *dressing perturbation theory* instead of pure perturbation theory under weak field to obtain the density-matrix elements [see Eqs. (A1)–(A7)] for the SPFWM fields (E_S and E_{aS})and FL signals based on the strong-field coupled equations.

The terms arising from collisional and vibrational interactions among ions or atoms cannot be conveniently included in a Hamiltonian description but, still, such interactions can lead to a change in the state of the system. Thus the last term in Eq. (A1) is added. The adiabatic residual particle transfer between states $|G_{1+}\rangle$ and $|G_{1-}\rangle$ (as described in Sec. IV) is attributed to phonon-assisted transition which is considered in the phenomenological term of our von Neumann equation.

Using the Liouville dynamics equation of motion in density-matrix form,

$$\frac{\partial\hat{\rho}(t)}{\partial t} = \frac{1}{i\hbar}[\hat{H},\hat{\rho}(t)] - \Gamma\hat{\rho}, \tag{A1}$$

where $\hat{H} = \hat{H}_0 + \hat{H}_1(t)$, $H_1 = -E\vec{\mu}$, and $\vec{\mu}$ is the transition dipole moment. H is the Hamiltonian; Γ is the population decay rate.

To obtain the density-matrix elements we may expand $\hat{\rho}(t)$ as

$$\hat{\rho}(t) = \hat{\rho}^{(0)}(t) + \hat{\rho}^{(1)}(t) + \hat{\rho}^{(2)} + \cdots + \hat{\rho}^{(r)}(t) + \cdots . \tag{A2}$$

Substituting (A2) into (A1) we obtain

$$\begin{aligned} &i\hbar\frac{\partial}{\partial t}[\hat{\rho}^{(0)}(t) + \hat{\rho}^{(1)}(t) + \hat{\rho}^{(2)} + \cdots + \hat{\rho}^{(r)}(t) + \cdots] \\ &\quad = [\hat{H}_0 + \hat{H}_1, \hat{\rho}^{(0)}(t) + \hat{\rho}^{(1)}(t) + \hat{\rho}^{(2)} + \cdots + \hat{\rho}^{(r)}(t) + \cdots] \\ &\qquad -i\hbar[\hat{\rho}^{(0)}(t) + \cdots + \hat{\rho}^{(r)}(t) + \cdots]. \end{aligned} \tag{A3}$$

Thus the above equation we will take the form

$$\begin{aligned} i\hbar\frac{\partial}{\partial t}\hat{\rho}^{(0)}(t) &= [\hat{H}_0, \hat{\rho}^{(0)}(t)] - i\hbar\Gamma[\hat{\rho}^{(0)}(t)], \\ i\hbar\frac{\partial}{\partial t}\hat{\rho}^{(1)}(t) &= [\hat{H}_0, \hat{\rho}^{(1)}(t)] + [\hat{H}_1, \hat{\rho}^{(0)}(t)] - i\hbar\Gamma\hat{\rho}^{(1)}(t), \\ i\hbar\frac{\partial}{\partial t}\hat{\rho}^{(r)}(t) &= [\hat{H}_0, \hat{\rho}^{(r)}(t)] + [\hat{H}_1, \hat{\rho}^{(r-1)}(t)] - i\hbar\Gamma\hat{\rho}^{(r)}(t). \end{aligned} \tag{A4}$$

Solving the above equations we get the density-matrix elements $\rho^{(0)} \cdots \rho^{(r)}$.

After solving the density-matrix dynamics equation, we obtain

$$\mu = \begin{bmatrix} 0 & \mu_1 & 0 & 0 \\ \mu_1 & 0 & \mu_2 & \mu_3 \\ 0 & \mu_2 & 0 & 0 \\ 0 & \mu_3 & 0 & 0 \end{bmatrix},$$

$$H_0 = \begin{bmatrix} E_0 & 0 & 0 & 0 \\ 0 & E_1 & 0 & 0 \\ 0 & 0 & E_2 & 0 \\ 0 & 0 & 0 & E_3 \end{bmatrix},$$

$$\hat{\rho}^{(r)} = \begin{bmatrix} \rho_{00}^{(r)} & \rho_{01}^{(r)} & \rho_{02}^{(r)} & \rho_{03}^{(r)} \\ \rho_{10}^{(r)} & \rho_{11}^{(r)} & \rho_{12}^{(r)} & \rho_{13}^{(r)} \\ \rho_{20}^{(r)} & \rho_{21}^{(r)} & \rho_{22}^{(r)} & \rho_{23}^{(r)} \\ \rho_{30}^{(r)} & \rho_{31}^{(r)} & \rho_{32}^{(r)} & \rho_{33}^{(r)} \end{bmatrix},$$

$$\Gamma\hat{\rho}^{(r)} = \begin{bmatrix} \Gamma_0\hat{\rho}_{00} & \Gamma_{10}\hat{\rho}_{01} & \Gamma_{20}\hat{\rho}_{02} & \Gamma_{30}\hat{\rho}_{03} \\ \Gamma_{10}\hat{\rho}_{10} & \Gamma_1\hat{\rho}_{11} & \Gamma_{21}\hat{\rho}_{12} & \Gamma_{31}\hat{\rho}_{13} \\ \Gamma_{20}\hat{\rho}_{20} & \Gamma_{21}\hat{\rho}_{21} & \Gamma_2\hat{\rho}_{22} & \Gamma_{32}\hat{\rho}_{23} \\ \Gamma_{30}\hat{\rho}_{30} & \Gamma_{31}\hat{\rho}_{31} & \Gamma_{32}\hat{\rho}_{32} & \Gamma_3\hat{\rho}_{33} \end{bmatrix}.$$

ρ_{lm} is the coherence between levels l and m.

To show the derivation as an example, let us consider the V-type three-level system. When two beams (E_1 and E_2) are turned on as in Fig. 1 (main text), a V-type three-level system ($|1\rangle \rightarrow |0\rangle \rightarrow |2\rangle$) is formed. The Hamiltonian of this system can be written as $H = -\hbar[\Delta_1|1\rangle\langle 1| + \Delta_2|2\rangle\langle 2|] - \hbar[G_1|1\rangle\langle 0| + G_2|2\rangle\langle 0| + \text{H.c.}]$. Then the density-matrix equations can be obtained by the Liouville equation:

$\frac{\partial}{\partial t}\rho = -\frac{i}{\hbar}[H,\rho] - \Gamma\rho.$

$$\frac{\partial \rho_{00}^{(r)}}{\partial t} = -\Gamma_{00}\rho_{00}^{(r)} + i\big[-G_2 e^{i\mathbf{k}_2\cdot\mathbf{r}}\tilde{\rho}_{02}^{(r-1)} + G_2^* e^{-i\mathbf{k}_2\cdot\mathbf{r}}\rho_{20}^{(r-1)} - G_1 e^{i\mathbf{k}_1\cdot\mathbf{r}}\rho_{01}^{(r-1)} + G_1^* e^{-i\mathbf{k}_1\cdot\mathbf{r}}\rho_{10}^{(r-1)}\big], \tag{A5}$$

$$\frac{\partial \rho_{10}^{(r)}}{\partial t} = -(i\Delta_1 + \Gamma_{10})\rho_{10}^{(r)} + i\big[-G_2 e^{i\mathbf{k}_2\cdot\mathbf{r}}\rho_{12}^{(r-1)} + G_1 e^{i\mathbf{k}_1\cdot\mathbf{r}}\big(\rho_{00}^{(r-1)} - \rho_{11}^{(r-1)}\big)\big], \tag{A6}$$

$$\frac{\partial \rho_{11}^{(r)}}{\partial t} = -\Gamma_{11}\rho_{11}^{(r)} + i\big[-G_1^* e^{-i\mathbf{k}_1\cdot\mathbf{r}}\rho_{10}^{(r-1)} + G_1 e^{i\mathbf{k}_1\cdot\mathbf{r}}\rho_{01}^{(r-1)}\big], \tag{A7}$$

$$\frac{\partial \rho_{20}^{(r)}}{\partial t} = -(i\Delta_2 + \Gamma_{20})\rho_{20}^{(r)} + i\big[G_2 e^{i\mathbf{k}_1\cdot\mathbf{r}}\big(\rho_{00}^{(r-1)} - \tilde{\rho}_{22}^{(r-1)}\big) - G_1 e^{i\mathbf{k}_1\cdot\mathbf{r}}\rho_{21}^{(r-1)}\big], \tag{A8}$$

$$\frac{\partial \rho_{12}^{(r)}}{\partial t} = -[i(\Delta_1 - \Delta_2) + \Gamma_{12}]\rho_{12}^{(r)} + i\big(G_2 e^{i\mathbf{k}_2\cdot\mathbf{r}}\rho_{10}^{(r-1)} - G_1^* e^{-i\mathbf{k}_1\cdot\mathbf{r}}\rho_{20}^{(r-1)}\big). \tag{A9}$$

Considering a V-type energy system, there is a simple SPFWM process expressed as the perturbation chain $\rho_{00}^{(0)} \xrightarrow{\boldsymbol{E}_1} \rho_{10}^{(1)} \xrightarrow{(\boldsymbol{E}_{S_1})^*} \rho_{00}^{(2)} \xrightarrow{\boldsymbol{E}_2} \rho_{20(E_{S_2})}^{(3)}$ and $\rho_{00}^{(0)} \xrightarrow{\boldsymbol{E}_2} \rho_{20}^{(1)} \xrightarrow{(\boldsymbol{E}_S)^*} \rho_{00}^{(2)} \xrightarrow{\boldsymbol{E}_1} \rho_{10(\mathrm{aS})}^{(3)}$. We would like to deduce the density-matrix elements of SPFWM (E_{S2}) in detail:

(i) In the first step, a ground-state particle $\rho_{00}^{(0)}$ absorbs a probe photon ε_1 and transits to state $\rho_{10}^{(1)}$, expressed as $\rho_{00}^{(0)} \xrightarrow{\varepsilon_1} \rho_{10}^{(1)}$ in the perturbation chain. From Eq. (A5), and under the weak-field ($iG_2^* e^{-i\mathbf{k}_2\cdot\mathbf{r}}\rho_{20} \approx 0$, $-iG_1 e^{i\mathbf{k}_1\cdot\mathbf{r}}\rho_{11} \approx 0$) and the steady-state ($\frac{\partial \rho_{10}}{\partial t}$=0) approximations, we can obtain $0 = -[i\Delta_1 + \Gamma_{10}]\rho_{10} + iG_1 e^{i\mathbf{k}_1\cdot\mathbf{r}}\rho_{00}$, namely,

$$\rho_{10}^{(1)} = \frac{iG_1 e^{i\mathbf{k}_1\cdot\mathbf{r}}}{i\Delta_1 + \Gamma_{10}}\rho_{00}^{0)}, \tag{A10a}$$

where the term $iG_1 e^{i\mathbf{k}_1\cdot\mathbf{r}}\rho_{00}$ remains because according to the perturbation chain $\rho_{00}^{(0)} \xrightarrow{\varepsilon_1} \rho_{10}^{(1)}$, only $iG_1 e^{i\mathbf{k}_1\cdot\mathbf{r}}\rho_{00}$ contributes to the process of generating FWM in the first step.

(ii) In the second step, the particle is stimulated back to the state ρ_{00} and emits a pumping photon ε_1^*, which is expressed as $\rho_{10}^{(1)} \xrightarrow{(\boldsymbol{E}_{\mathrm{aS}})^*} \rho_{00}^{(2)}$. From Eq. (A5), and under the approximations of weak field and steady state, we have $0 = -\Gamma_{00}\rho_{00}^{(r)} + iG_1^* e^{-i\mathbf{k}_1\cdot\mathbf{r}}\rho_{10}^{(r-1)}$, namely,

$$\rho_{00}^{(2)} = \frac{iG_1^* e^{-i\mathbf{k}_{E_{\mathrm{S}}1}\cdot\mathbf{r}}}{\Gamma_{00}}\rho_{10}^{(1)}. \tag{A10b}$$

(iii) In the third step, the particle absorbs a pumping photon ε_2 and transits to the dressed state $\rho_{20(\mathrm{S})}^{(3)}$, which can be expressed as $\rho_{00}^{(2)} \xrightarrow{\boldsymbol{E}_2} \rho_{20(\mathrm{S})}^{(3)}$. From Eq. (A8), and under the approximations of weak field and steady state, it becomes $0 = -(i\Delta_2 + \Gamma_{20})\rho_{20}^{(3)} + iG_2 e^{i\mathbf{k}_2\cdot\mathbf{r}}\rho_{00}^{(2)}$, and then

$$\rho_{20}^{(3)} = \frac{iG_2 e^{i\mathbf{k}_2\cdot\mathbf{r}}}{i\Delta_2 + \Gamma_{20}}\rho_{00}^{(2)}. \tag{A10c}$$

Substituting Eq. (A10a) into Eq. (A10b), and then putting the result into Eq. (A10c), under the approximation of $\rho_{00}^{(0)} \approx 1$, we get

$$\rho_{10}^{(3)} = \frac{iG_1 G_{E_{\mathrm{S}}1}^* G_2 e^{i(\mathbf{k}_1+\mathbf{k}_2-\mathbf{k}_{E_{\mathrm{S}}1})\cdot\mathbf{r}}}{(i\Delta_1 + \Gamma_{10})\Gamma_{00}(i\Delta_2 + \Gamma_{20})}. \tag{A11}$$

When a strong dressing field is added on the above state $|0\rangle$, the dressed FWM signals are generated. The perturbation chain can then be written as the dressed perturbation chain: $\rho_{00}^{(0)} \xrightarrow{\boldsymbol{E}_1} \rho_{1G_{2\pm}}^{(1)} \xrightarrow{(\boldsymbol{E}_{S_1})^*} \rho_{G_{2\pm}0}^{(2)} \xrightarrow{\boldsymbol{E}_2} \rho_{20(E_{\mathrm{aS}_1})}^{(3)}$. On the other hand, the perturbation approach for such dressing cases can be well described by the following coupled equations:

$$\left.\begin{aligned} 0 &= -(i\Delta_1 + \Gamma_{10})\rho_{10}^{(1)} - iG_2 e^{i\mathbf{k}_2\cdot\mathbf{r}}\rho_{12} + iG_1 e^{i\mathbf{k}_1\cdot\mathbf{r}}\rho_{00}^{(0)} \\ 0 &= -[i(\Delta_1 - \Delta_2) + \Gamma_{12}]\rho_{12} + iG_2 e^{-i\mathbf{k}_2\cdot\mathbf{r}}\rho_{10}^{(r-1)} \end{aligned}\right\}, \text{ (coupling equations).}$$

In the steady state, we have

$$\rho_{10}^{(1)} = \frac{iG_1 e^{i\mathbf{k}_1\cdot\mathbf{r}}}{i\Delta_1 + \Gamma_{10} + \frac{|G_2|^2}{i(\Delta_1-\Delta_2)+\Gamma_{12}}}\rho_{00}^{(0)}.$$

Similarly,

$$\rho_{00}^{(2)} = \frac{iG_1^* e^{-i\mathbf{k}_1\cdot\mathbf{r}}}{\Gamma_{00} + \frac{|G_2|^2}{i\Delta_2+\Gamma_{20}}}\rho_{10}^{(1)}.$$

We can finally obtain

$$\rho_{20(E\mathrm{aS}_1)}^{(3)} = \frac{iG_1 G_{\mathrm{aS}}^* G_2 e^{i(\mathbf{k}_1+\mathbf{k}_2-\mathbf{k}_{E_{\mathrm{S}}1})\cdot\mathbf{r}}}{\big[i\Delta_1 + \Gamma_{10} + \frac{|G_2|^2}{i(\Delta_1-\Delta_2)+\Gamma_{12}}\big]\big[\Gamma_{00} + \frac{|G_2|^2}{i\Delta_2+\Gamma_{20}}\big]}\frac{1}{(i\Delta_2 + \Gamma_{20})}. \tag{A12}$$

By applying field E_1 to modify such a process, the output signal can be given as

$$\rho^{(3)}_{20(E\mathrm{aS}_1)} = \frac{iG_1G^*_{\mathrm{aS}}G_2e^{i(\mathbf{k}_1+\mathbf{k}_2-\mathbf{k}_{E\mathrm{S}1})\cdot\mathbf{r}}}{\left[i\Delta_1+\Gamma_{10}+\frac{|G_2|^2}{i(\Delta_1-\Delta_2)+\Gamma_{12}}+\frac{|G_2|^2}{\Gamma_{00}}\right]\left[\Gamma_{00}+\frac{|G_2|^2}{i\Delta_2+\Gamma_{20}}\right]}\frac{1}{(i\Delta_2+\Gamma_{20})}. \tag{A13}$$

[1] A. Einstein, B. Podolsky, and N. Rosen, Phys. Rev. **47**, 777 (1935).
[2] H. J. Kimble, Nature **453**, 1023 (2008).
[3] R. Hanbury-Brown and R. Q. Twiss, Nature **177**, 27 (1956).
[4] J. D. Cresser, J. Phys. B: At. Mol. Phys. **20**, 4915 (1987).
[5] L. Knoll, W. Vogel, and D.-G. Welsch, Phys. Rev. A **36**, 3803 (1987).
[6] E. del Valle, A. Gonzalez-Tudela, F. P. Laussy, C. Tejedor, and M. J. Hartmann, Phys. Rev. Lett. **109**, 183601 (2012).
[7] A. Christ, C. Lupo, M. Reichelt, T. Meier, and C. Silberhorn, Phys. Rev. A **90**, 023823 (2014).
[8] S.-Y. Lan, S. D. Jenkins, T. Chanelière, D. N. Matsukevich, C. J. Campbell, R. Zhao, T. A. B. Kennedy, and A. Kuzmich, Phys. Rev. Lett. **98**, 123602 (2007).
[9] A. V. Turukhin, V. S. Sudarshanam, M. S. Shahriar, J. A. Musser, B. S. Ham, and P. R. Hemmer, Phys. Rev. Lett. **88**, 023602 (2001).
[10] J. J. Longdell, E. Fraval, M. J. Sellars, and N. B. Manson, Phys. Rev. Lett. **95**, 063601 (2005).
[11] A. Kuzmich, W. P. Bowen, A. D. Boozer, A. Boca, C. W. Chou, L.-M. Duan, and H. J. Kimble, Nature **423**, 731 (2003).
[12] H. Lan, C. Li, C. Lei, H. Zheng, R. Wang, M. Xiao, and Y. Zhang, Laser Phys. Lett. **12**, 015404 (2015).
[13] Y. Zhang, U. Khadka, B. Anderson, and M. Xiao, Phys. Rev. Lett. **102**, 013601 (2009).
[14] Y. Zhang, Z. Wang, Z. Nie, C. Li, H. Chen, K. Lu, and M. Xiao, Phys. Rev. Lett. **106**, 093904 (2011).
[15] R. Z. Vered, Y. Shaked, Y. Ben-Or, M. Rosenbluh, and A. Pe'er, Phys. Rev. Lett. **114**, 063902 (2015).
[16] Z. Z. Qin, L. M. Cao, H. L. Wang, A. M. Marino, W. P. Zhang, and J. T. Jing, Phys. Rev. Lett. **113**, 023602 (2014).
[17] P. van Loock, T. D. Ladd, K. Sanaka, F. Yamaguchi, K. Nemoto, W. J. Munro, and Y. Yamamoto, Phys. Rev. Lett. **96**, 240501 (2006).
[18] H. Jeong, A. Zavatta, M. Kang, S.-W. Lee, L. S. Costanzo, S. Grandi, T. C. Ralph, and M. Bellini, Nat. Photonics **8**, 564 (2014).
[19] R. W. Equall, R. L. Cone, and R. M. Macfarlane, Phys. Rev. B **52**, 3963 (1995).
[20] M. D. Lukin, A. B. Matsko, M. Fleischhauer, and M. O. Scully, Phys. Rev. Lett. **82**, 1847 (1999).
[21] H. X. Chen, M. Z. Qin, Y. Q. Zhang, X. Zhang, F. Wen, J. M. Wen, and Y.P. Zhang, Laser Phys. Lett. **11**, 045201 (2014).
[22] V. Boyer, A. M. Marino, R. C. Pooser, and P. D. Lett, Science **321**, 544 (2008).
[23] J. F. Clauser, Phys. Rev. D **9**, 853 (1974).